ICOSSAR 2021
The 13th International Conference on Structural Safety and Reliability (ICOSSAR 2021), June 21-25, 2021, Shanghai, P.R. China
J. Li, Pol D. Spanos, J.B. Chen & Y.B. Peng (Eds)

Exploiting the peak deformation-hysteretic energy relationship in aftershock fragility analysis

Roberto Gentile[a] and Carmine Galasso[b]

[a] *Institute for Risk and Disaster Reduction & Department of Civil, Environmental and Geomatic Engineering. University College London.* r.gentile@ucl.ac.uk
[b] *Department of Civil, Environmental and Geomatic Engineering, University College London & Scuola Universitaria Superiore (IUSS) Pavia.* c.galasso@ucl.ac.uk

ABSTRACT: A recently-proposed framework to derive state-dependent fragility relationship of structures subjected to ground-motion sequences (e.g. mainshock-aftershock or triggered earthquakes) is illustrated. The hysteretic energy dissipated in the sequence is adopted as the main engineering demand parameter (EDP) since it is a cumulative measure that monotonically increases with the excitation length. According to the framework, the hysteretic energy-peak deformation trend is estimated and used to convert deformation-based EDP damage-state thresholds into energy-based ones. A vector-valued probabilistic seismic demand model is derived in the form of a surface relating the hysteretic energy in the sequence to the peak deformation in the mainshock and a ground-motion intensity measure of the aftershock. This is calibrated via sequential cloud-based time-history analyses. Finally, state-dependent fragility curves are derived. The framework is demonstrated for 14 reinforced concrete frame buildings with different heights, plastic mechanisms and infill distribution. The results show the feasibility of the proposed approach, effectively capturing damage accumulation without inconsistencies in the obtained statistical model.

KEYWORDS: ground-motion sequences; mainshock-aftershock; seismic fragility; hysteretic energy vs peak deformation; probabilistic seismic demand model; reinforced concrete frames.

1 INTRODUCTION AND MOTIVATION

In seismic design or performance assessment of structures, peak quantities (mainly displacement or drift) are generally adopted to define demands and capacities at a global or member level. However, disregarding cumulative engineering demand parameters, EDPs (e.g. hysteretic energy, cumulated ductility demand, number of cycles) may not provide an analyst with the complete control of the performance assessment process under certain circumstances in which low-cycle fatigue is relevant (Fajfar, 1992; Cosenza and Manfredi, 2000). Among those, this paper deals explicitly with ground-motion sequences in which a first ground motion (called mainshock, MS) is followed by a second one (called aftershock, AS, for simplicity), which can either be an actual aftershock or a record related to a triggered event.

Some recent research attention has been devoted to developing a fragility relationship for MS-AS ground motion sequences that explicitly depend on the damage state (DS) achieved by a structure in the MS (i.e. state-dependent fragility). Most studies derive seismic fragility in terms of maximum inter-storey drift thresholds (e.g. (Aljawhari, Freddi and Galasso, 2019; Di Trapani and Malavisi, 2019; Papadopoulos, Kohrangi and Bazzurro, 2020)), although in some cases this is considered in conjunction with the residual drift (e.g. (Zhang et al., 2020)). This may create inconsistencies in the resulting statistical models due to inappropriate consideration of damage accumulation. For instance, if the peak drift computed for an AS ground motion is smaller than the one due to the corresponding MS, the structure is allocated to a lower DS with

respect to that of the MS, which is inconsistent. This can, in turn, result in fragility curve crossings between various damage states). Since hysteretic energy is a cumulative measure that monotonically increases with the length of the applied excitation (see Changhai et al., (2018), for example), the inconsistency mentioned above is automatically removed if hysteretic energy is used as an EDP.

Several studies explicitly included cumulative EDPs in the design/assessment process (Housner, 1956; Uang and Bertero, 1990; Fajfar, 1992; Malhotra, 2002; Kunnath and Chai, 2004; Chai, 2005). In a recent paper (Gentile and Galasso, 2021), the authors proposed a framework to 1) define reliable DS thresholds in terms of hysteretic energy; 2) derive a PSDM in the form of a surface relating the hysteretic energy in the MS-AS sequence to the peak deformation in the MS and a ground-motion intensity measure (IM) of the AS; 3) calculate state-dependent fragility relationships (i.e. representing the exceeding probability of a DS in the AS, conditioned on the IM of the AS, and the DS in the MS) using hysteretic energy as the selected EDP.

The present paper reviews the framework mentioned above and demonstrates it for 14 reinforced concrete (RC) frame buildings.

2 PEAK DEFORMATION VS HYSTERETIC ENERGY

For a structure subjected to dynamic excitation, the energy dissipated through hysteresis (or hysteretic energy) depends on the force-deformation backbone curve of the system and a set of hysteretic rules. The backbone curve describes the (tangent) system's stiffness under monotonic, quasi-static loading, whereas the hysteresis describes how such stiffness evolves under cyclic conditions, i.e. under unloading and reloading conditions. More complete models also involve strength degradation, both within a single cycle or across multiple cycles. Within-cycle degradation depends on the maximum deformation (or ductility) demand and modifies the backbone curve (usually corresponding to a negative slope). Cyclic degradation generally depends on the number of plastic excursions (i.e. when the response "leaves" the backbone curve). The combination of the parameters mentioned above, together with the applied load history (e.g. a ground motion), determines the amount of hysteretic energy dissipated by a structure. The amount of viscous damping significantly affects the hysteretic energy, i.e. the higher the damping, the lower the hysteretic energy.

For a realistic structure, damping depends on both material and lateral resisting system (e.g. steel frame vs RC wall). Moreover, the modal properties of the structure affect hysteretic energy, especially if higher modes are relevant. Therefore, for a given material/lateral-load resisting system, this is indirectly controlled by the structure's height. Most importantly, the plastic mechanism is a fundamental factor to consider, which is likely governed by the level of seismic design. This affects the members involved in the non-linear dynamic response, and therefore both the monotonic and cyclic properties at the global level.

Based on this discussion, any consideration about hysteretic energy cannot be generalised. However, for a given (archetype) structure, the ground motion record is the most relevant parameter to consider when characterising the energy-vs-deformation relationship.

For single ground-motion conditions, there exists a stable, pseudo-parabolic relationship between the global peak displacement and the hysteretic energy of a system (Decanini, Mollaioli and Saragoni, 2000; Terán Gilmore, 2001; Quinde, Terán-Gilmore and Reinoso, 2019).

Gentile and Galasso (2021) generalised this discussion by considering mainshock-aftershock conditions and adopting SDoF systems and frame structures. For a given value of the aftershock maximum deformation, there is a decreasing relationship between the hysteretic energy in the AS and the peak deformation in the MS. Therefore, a structure dissipates less energy (for a given peak deformation in the AS) if the dissipation in the MS is higher (which is proportional to the peak MS deformation).

This is shown here for a realistic RC frame. The details of the case study (discussed in Section 4.1) are deemed less relevant here. The frame is analysed via a cloud-based approach using 1000 MS-AS sequences obtained randomly assembling natural ground-motion records (Section 3.1). Figure 1.a shows the results of the analyses in terms of hysteretic energy ($E_{H,MS}$) vs maximum inter-storey drift for MSs only (θ_{MS}). The proposed law $E_{H,MS} = a\theta_{\mathrm{MS}}^{b}$ is fitted to the obtained data. This curve is used to define

energy-based DS thresholds starting from drift-based ones (as discussed in detail in Section 3.2). The $E_{H,AS}$ vs θ_{AS} data is partitioned based on the DS achieved in the MS, and further power-law models are fitted to each subset of data. They are shown in Figure 1.b, in which only the points related to DS2 in the MS are shown to improve the clarity of the plot. It is worth mentioning that the AS drift is calculated relatively to the residual MS drift. The results clearly show that for a given value of θ_{AS}, the $E_{H,AS}$ values are lower for a higher DS in the MS (corresponding to a higher $E_{H,MS}$ and θ_{MS}). It is worth repeating that the absolute value of the fitting parameters (a, b) strongly depends on the backbone, hysteresis and degradation properties of the considered structure, in turn dependent on the material, lateral-load resisting system, dynamic properties, etc.

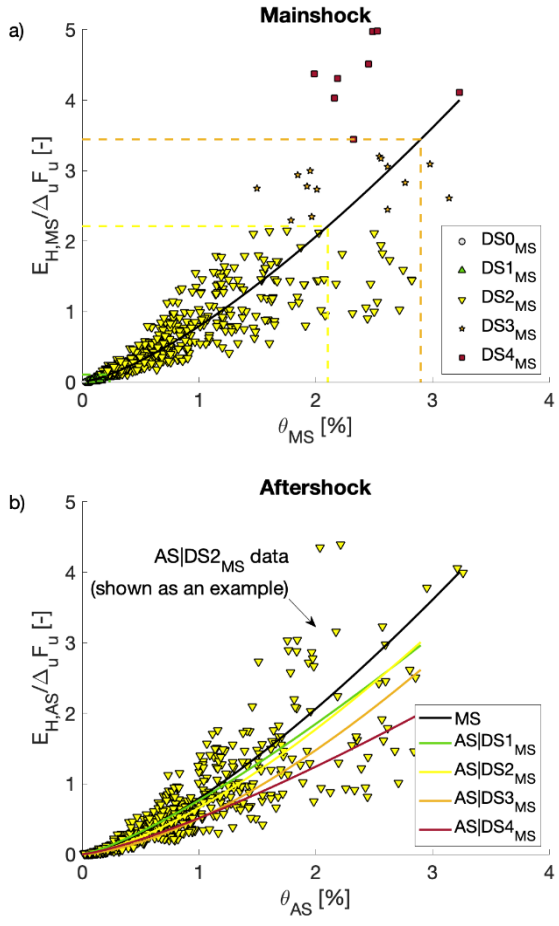

Figure 1. Hysteretic energy vs maximum inter-storey drift relationship for a case-study RC frame: a) mainshock; b) aftershock (dependent on the damage state in the mainshock). Gentile and Galasso (2021)

3 FRAMEWORK TO DERIVE STATE-DEPENDENT FRAGILITY

The described procedure for state-dependent fragility analysis is based on a cloud-based approach to NLTHAs using ground motion sequences composed of two real (i.e. recorded) ground motions (herein called MS and AS, for simplicity). For each considered sequence, the maximum inter-storey drift and the hysteretic energy are registered in both the MS and AS. Such data is used to calibrate a 5-parameter PSDM represented by a surface depending on the maximum response in the MS and the IM of the AS.

For any set of drift-based DS thresholds (selected by the user), the above PSDM is used to derive the corresponding thresholds based on the (normalised) hysteretic energy. It is assumed that the energy-based thresholds remain unchanged regardless of the demand in the aftershock. A set of lognormal fragility relationships is fitted: for the undamaged structure (using the hysteretic energy in the mainshock as an EDP) and for each considered DS in the mainshock (using the sum of the mainshock-aftershock hysteretic energy).

3.1 *Assembled ground-motion sequences*

A randomised approach based on real records is adopted to obtain ground-motion sequences, as done in Aljawhari et al. (2019). The seed ground motions (crustal only) used for this process are described in detail in Gentile and Galasso (2021). By separately considering both horizontal components of the seed records (MS only), 626 ground motions are selected.

By combining two records (MS and AS), artificial sequences are assembled, allowing 40s of free vibration in between. Instead of considering all the possible combinations (391,876), 1000 random pairs are selected adopting the Latin hypercube sampling (LHS) approach. The details of this process are described in detail in Gentile and Galasso (2021).

Figure 2 illustrates the geometric mean of the 5%-damped pseudo-spectral acceleration in a range of periods ($AvgSA$) for the MS and AS in each sequence. The range of periods [0.2s-1.8s] is herein selected for illustration purposes only. This randomised selection method reduces the computational burden for the NLTHAs, while keeping a wide variety of low and high IM levels

for both MS and AS.

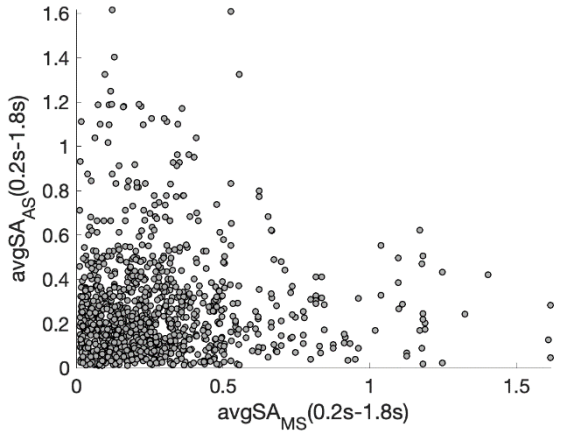

Figure 2. Randomly selected 1000 sequences via the Latin hypercube sampling approach. Modified after Gentile and Galasso (2021)

3.2 *Probabilistic seismic demand model*

The described PSDM is the surface $E_{H,MSAS}(\theta_{MS}, IM_{AS})$, where θ_{MS} is the maximum inter-storey drift in the MS and IM_{AS} is an intensity measure in the AS (e.g. $AvgSA$). The functional form of the PSDM is given in Equations 1 and 2, in which the MS and AS hysteretic energy values are treated separately and then summed. The model depends on five parameters (a, b, c_0, d, m), estimated through regressions.

$$\begin{aligned} E_{H,MSAS} &= E_{H,MS} + E_{H,AS} \\ &= a\theta_{MS}^{b} + c(\theta_{MS})IM_{AS}^{d} \end{aligned} \quad (1)$$

$$c(\theta_{MS}) = (1 - m\theta_{MS})c_0 \quad (2)$$

Figure 3.a shows the MS portion of the hysteretic energy, together with an example scatter of the MS data. These data lie in the $(\theta_{MS}, E_{H,MS})$ plane and it may be fitted with the power law relationship $a\theta_{MS}^{b}$. Such relationship is monotonically increasing as a function of θ_{MS} and constant as a function of IM_{AS}. Figure 3.b, on the other hand, shows the AS portion of the hysteretic energy together with the AS scatter data $(\theta_{MS}, IM_{AS}, E_{H,AS})$. In the $(IM_{AS}, E_{H,AS})$ plane, the mainshock data is also shown (therefore for $\theta_{MS} = 0$). This is possible considering that a MS can be interpreted as an AS that follows an MS producing zero drift (i.e. an AS that follows no MS is the MS itself). This consideration allows calibrating the relationship $E_{H,MSAS}(\theta_{MS} = 0) = c_0 IM_{AS}^{d}$ using the MS data only. In this way, using this PSDM for MS-only predictions will provide, by definition, the same result as the simple power-law model used in single-record conditions.

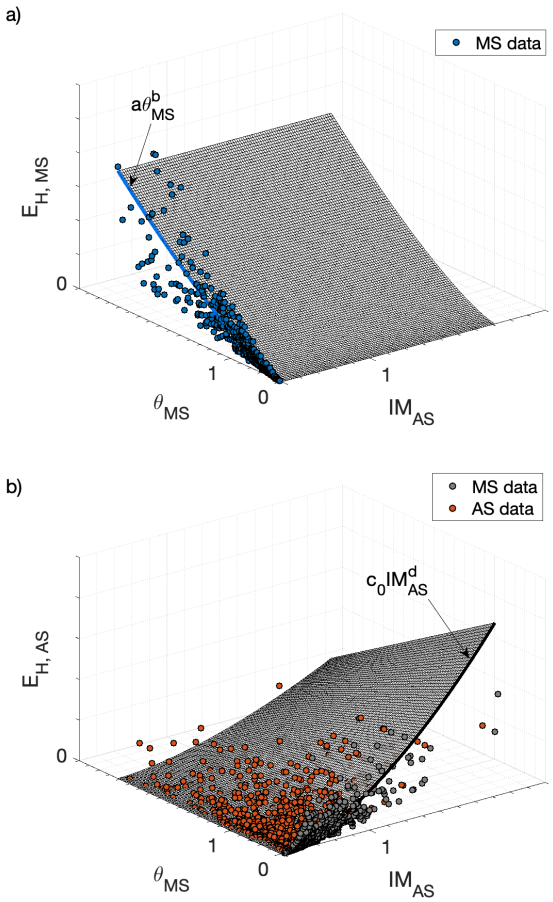

Figure 3. Derivation of the probabilistic seismic demand model: a) mainshock; b) aftershock. Gentile and Galasso (2021)

Finally, the factor $c(\theta_{MS}) = (1 - m\theta_{MS})c_0$ allows to linearly reduce the "slope" of the $c_0 IM_{AS}^{d}$ relationship as a function of θ_{MS}. This function is fitted using the AS data $(\theta_{MS}, IM_{AS}, E_{H,AS})$. It is worth mentioning that the dynamic analyses leading to "collapse" are herein disregarded and the information carried out by such data can be considered when deriving the fragility relationships. Collapse herein corresponds to a global dynamic instability of the numerical analysis (i.e. non-convergence), likely corresponding to a plastic mechanism (i.e. the structure is under-determined) or exceeding a conventional 10% maximum inter-storey drift.

The steps to fit the proposed PSDM are herein resumed:

1. Using the mainshock data only

($\theta_{MS}, E_{H,MS}$), the relationship $a\theta_{MS}^{b}$ is fitted. The parameters a and b are estimated via the linear least-squares method in the log-log space (i.e. $lnE_{H,MS} = aln\theta_{MS} + b$);

2. Using the mainshock data only ($IM_{MS}, E_{H,MS}$), the relationship $c_0 IM_{AS}^{d}$ is fitted. The parameters c_0 and d are estimated as per point 1;
3. Using the AS data ($\theta_{MS}, IM_{AS}, E_{H,AS}$), the parameter m is estimated via the non-linear least squares to the function $E_{H,AS} = (1 - m\theta_{MS})c_0 IM_{AS}^{d}$.

3.3 *State-dependent fragility analysis*

The proposed PSDM is used to derive state-dependent fragility relationships in the form of lognormal cumulative distribution functions (CDFs). As shown in Figure 4.a (Mixed-sway 4 storey case study, below), after selecting the drift thresholds ($\overline{\theta_{DS}}$) for an arbitrary number N of DSs, the PSDM itself will automatically provide their conversion in terms of hysteretic energy thresholds ($\overline{E_{H,DS}}$). Eq. 3 allows deriving fragility curves for different combinations of the DS in both the MS and AS, specified as $F(DS_{AS}|DS_{MS})$. Practically, $F(ds|0)$ are the MS fragilities (with $ds = 1 \dots N$), while $F(DS_{AS}|DS_S)$ represent the AS fragility conditioned on a given DS in the MS. In the latter condition, $DS_{AS} = DS_{MS} + 1 \dots N$, i.e. they represent the exceeding probability of the aftershock causing a "jump" to a higher DS with respect to the MS, conditioned to IM_{AS}. In such equation, $\mu_{lnE_H|DS_{MS},IM_{AS}}$ is the fragility median (also called $\mu(DS_{AS}|DS_{MS})$, for simplicity) while $\sigma_{lnE_H|DS_{MS},IM_{AS}}$ is the logarithmic standard deviation.

$$F(DS_{AS}|DS_{MS}) = P\left(E_H \geq \overline{E_{H,DS_{AS}}} \middle| DS_{MS}, IM_{AS}\right) = 1 - \Phi\left(\frac{ln\overline{E}_{H,DS_{AS}} - \mu_{lnE_H|DS_{MS},IM_{AS}}}{\sigma_{lnE_H|DS_{MS},IM_{AS}}}\right) \quad (3)$$

Using the drift threshold for DS_{MS} and the energy threshold for DS_{AS}, and inverting Eq. 1, the median of a given fragility curve is calculated (Eq. 4). Eq. 5 provides the fragility relationships' dispersion, starting from the logarithmic standard deviation (from the PSDM). The resulting fragility relationships are shown in Figure 4.b. As a direct consequence of having a monotonically-increasing PSDM, the median of the AS fragility curves, for a given DS_{AS}, decreases as DS_{MS} increases. This means that damage accumulation is captured in a consistent and physically-sound fashion.

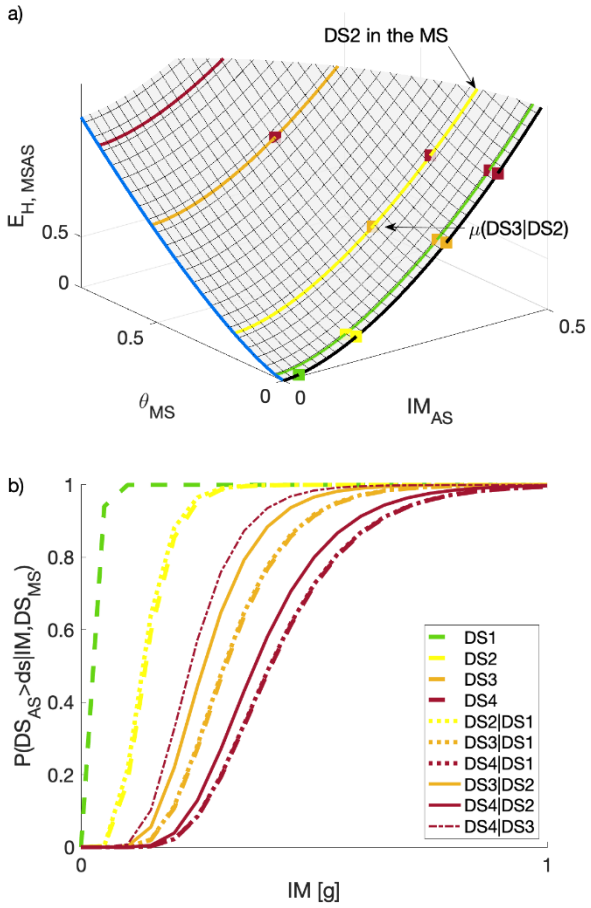

Figure 4. a) probabilistic seismic demand model; b) state-dependent fragility functions. Gentile and Galasso (2021)

It is worth repeating that the information carried out by the "collapse" analysis cases (dynamic instability or exceeding 10% drift), initially not considered in fitting the PSDM, can be accounted for here. Although this is not done here for simplicity, the probability of collapse can be represented by a generalised regression model with a "logit" link function (logistic regression), which is appropriate for cases in which the response variable is binary (in this case, "collapse" or "no collapse"). Then, the total probability theorem can be used to modify any of the calculated fragility curves.

$$\mu_{lnE_H|DS_{MS},IM_{AS}} = \mu(\mathrm{DS_{AS}}|\mathrm{DS_{MS}}) = \left(\frac{\overline{E_{H,DS_{AS}}} - a\overline{\theta^{b}_{DS_{MS}}}}{c_0(1 - m\overline{\theta_{DS_{MS}}})}\right)^{1/d} \quad 4$$

$$\beta = \sigma_{lnE_H|DS_{MS},IM_{AS}}/\mathrm{d} \quad 5$$

4 ILLUSTRATIVE APPLICATION

4.1 *Selected Case Studies*

14 RC frames case studies (Figure 5) are selected for illustrative purposes. They have four bays and either four or eight storeys. For each geometrical configuration, three different solutions are adopted for the seismic design and detailing of the RC members, leading to three different expected plastic mechanisms: beam sway (all beams and the base columns yield), mixed sway (combination of joint shear failures with beam and/or column flexure, shear or lap-splice failures) and column sway (soft storey mechanism at ground storey). Capacity design principles are ensured for these frames, also including the minimum requirements for structural details according to the New Zealand design standards (NZS3101, 2006). The Mixed-Sway frames have similar strength with respect to the Beam-Sway ones, but they do not meet any minimum requirement for the structural details. This leads to a similar peak base shear in the pushover curve but a considerably lower ductility capacity. The Column-Sway frames are designed for gravity loads only. The reader is referred to Gentile et al. (2019) for details on the design of the case studies, the member detailing of each RC member, the adopted material models, the load analysis and mass properties.

For each plastic mechanism configuration, both a bare and a uniformly-infilled configuration is considered. Finally, a pilotis configuration (infills missing at the ground floor) is also considered for the column-sway cases. Such case studies could also be considered as "archetype" structures representative of different vulnerability classes in various earthquake-prone regions of the world.

State-of-the-art non-linear time-history analyses are carried out for refined 2D numerical models defined using the finite element software Ruaumoko (Carr, 2016). The lumped plasticity-based modelling strategy (described in detail in Gentile and Galasso, 2021) explicitly accounts for the most probable failure mechanisms of RC beams and columns, such as flexure, bar buckling, lap-splice failure and shear. The non-linear behaviour of beam-column joint panels is considered via calibrated springs, while infills are modelled via a strut-based approach. Details about the adopted hysteretic rules and strength degradation (both within-cycle and cyclic) are given in Gentile and Galasso (2021).

Four structure-specific DSs are assumed to derive fragility curves: slight, moderate, extensive and complete damage (DS1 to DS4). Those DSs are qualitatively defined according to HAZUS, HAZard United States (Kircher, Whitman and Holmes, 2006), and quantified for each case study using the pushover analyses results for each analysed model. The plastic mechanisms of the four-storey frames, measured at the onset of DS3, are shown in Figure 5.

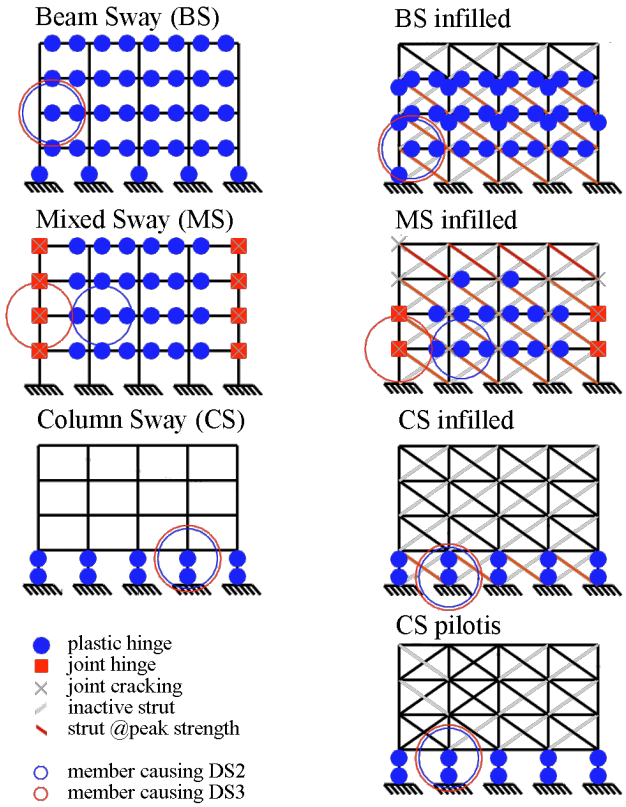

Figure 5. Plastic mechanism (DS3) for the analysed case studies. For each case study, there is an 8-storey one with a similar plastic mechanism. Modified after Gentile and Galasso (2021)

4.2 *Discussion*

Figure 6.a shows the pushover curves for all the considered case studies. Those are represented in terms of displacement at the effective height (Priestley et al., 2007) and base shear normalised with respect to the total weight. It is clear how the four-storey frames are consistently stronger than

the corresponding eight-storey ones while having a higher DS4 displacement. The mixed-sway frames have a slightly smaller strength with respect to the corresponding beam-sway ones while having a substantially lower displacement at DS4. The column-sway case studies show a particularly low strength and deformation capacity, together with a remarked degrading behaviour. For the beam- and mixed-sway frames, the degrading behaviour starts at particularly large displacements. As expected, the presence of the infills causes both a strength and stiffness increase for small displacements, followed by a sudden drop due to their pronounced degrading behaviour. The pilotis column-sway frames show practically the same behaviour as the column-sway bare ones.

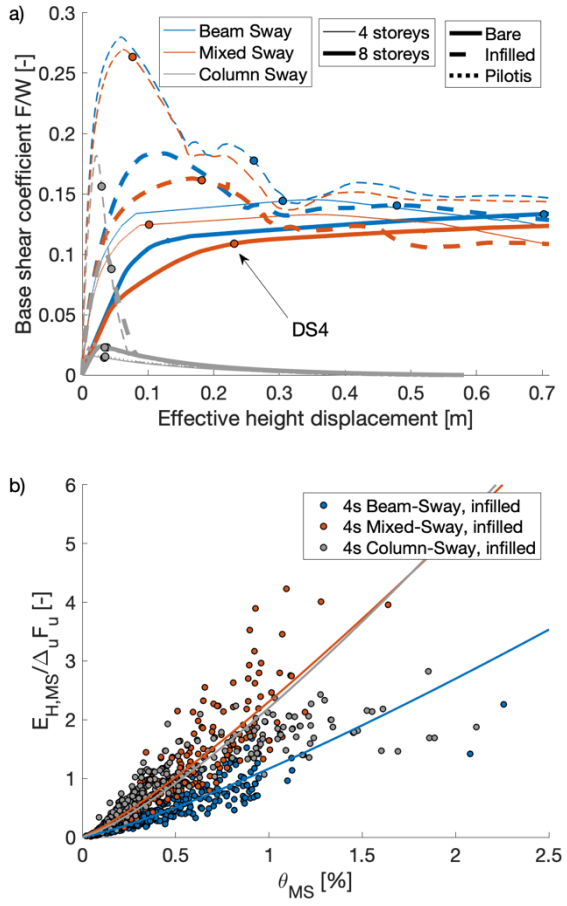

Figure 6. a) Normalised pushover curves. F: base shear, W: total weight; b) Normalised hysteretic energy vs maximum inter-storey drift for the four-storey infilled case studies. Δ_u, F_u: displacement and base shear at damage state 4. Gentile and Galasso (2021)

Figure 6.b shows the hysteretic energy vs maximum inter-storey drift scatter for the four-storey infilled frames (beam-, mixed- and column-sway). The hysteretic energy is normalised with respect to the product of the base shear and displacement at DS4 (called $F_u\Delta_u$).

The degrading behaviour of the case studies has a pronounced effect on the hysteretic energy vs maximum inter-storey drift relationship. Indeed, such a relationship has an asymptotic behaviour for the shown column-sway case, unlike the beam- and mixed-sway frames, which show a considerably lower degradation (within the range of the analysed drift values). Such an asymptotic behaviour is also theoretically expected for beam- and mixed-sway frames, although this would emerge for unphysically-large values of the drift.

Figure 7 shows the fragility curves for the four-storey beam-, mixed- and column-sway bare frames, together with the mixed-sway, infilled one. Both the PSDMs and the fragility curves are derived by adopting $avgSA$ as an IM. In particular, $avgSA$ is calculated in the range $[0.2T_1 - 1.5T_1]$ for the bare frames (including the column-sway, pilotis ones) and $[0.2T_1 - 3.0T_1]$ for the infilled frames.

As expected, for all the case studies, a low level of damage (DS1) does not cause a shift of the AS fragilities for all the other DSs. However, higher levels of damage (DS2 or DS3) have different effects depending on the considered case study. As expected, the beam-sway frames are only slightly affected by damage accumulation, likely due to their remarkably stable hysteresis governed by the flexure in the beams. As shown in Figure 7.a, a higher DS in the MS essentially caused no shift in the AS fragility medians. The only exception is the DS4 median given DS3 in the MS. Although this corresponds to a 25% reduction of the DS4 fragility median for the MS, this is unlikely to be relevant for practical purposes. First, because the DS4|DS3 median is still sufficiently high. Moreover, if such a structure experiences a DS3 due to the MS, it is likely to be tagged unsafe to occupy in the aftermath of the MS.

On the other hand, column-sway frames (Figure 7.c) are considerably affected by damage accumulation, given their unstable hysteretic behaviour and the pronounced strength degradation. The DS3 fragility median in the MS is reduced by 30% if DS2 is registered in the MS

(DS3|DS2 fragility). The reduction is equal to 47% for the DS4|DS3 fragility. In absolute terms, however, this effect corresponds to a small reduction in the median capacity since the MS fragilities of this type of uncompliant buildings (exhibiting a soft-storey behaviour) is particularly low. Therefore, damage accumulation may be practically less relevant in this case, as these types of structures are likely to sustain a large DS in the MS and likely be tagged as unsafe.

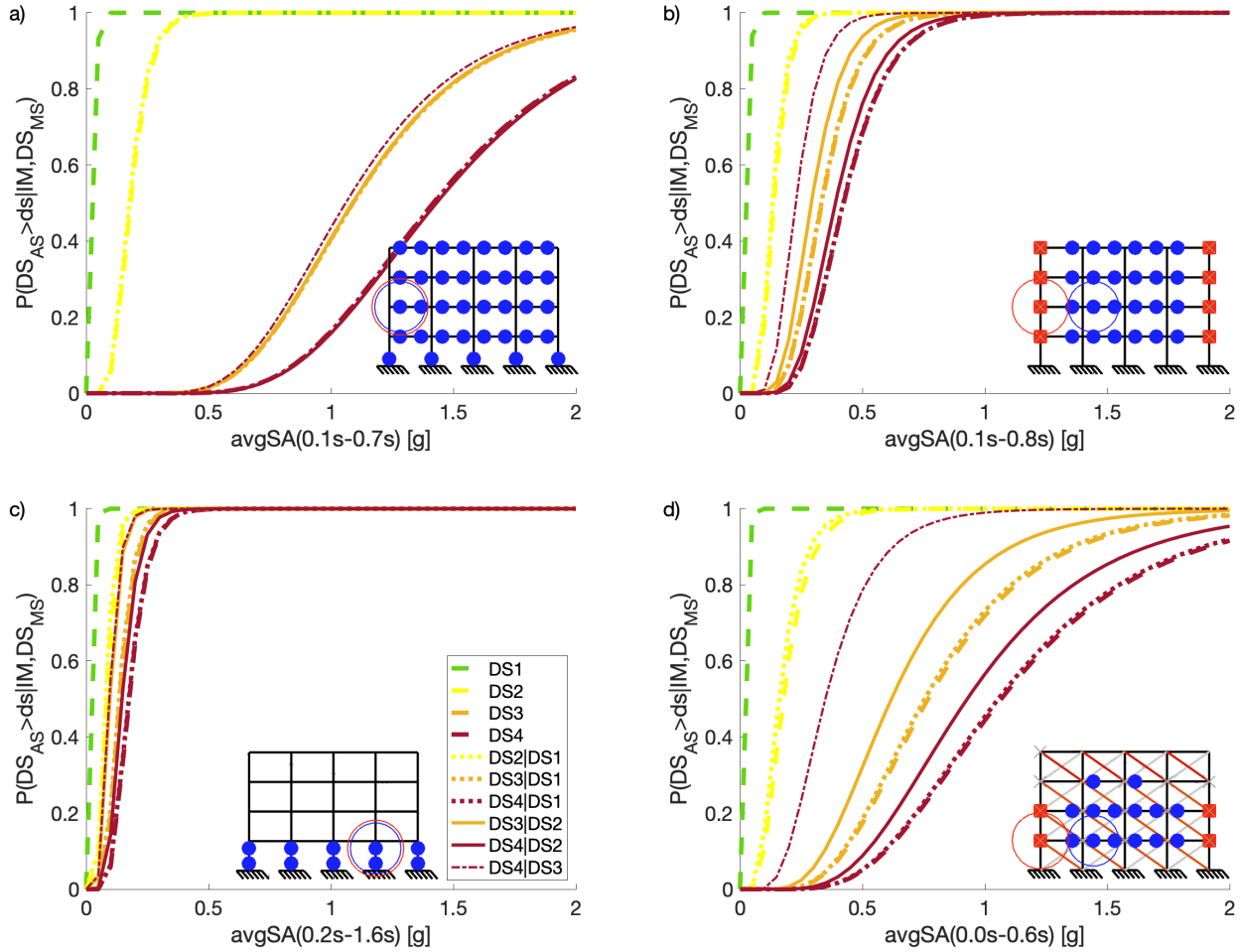

Figure 7. State-dependent fragility (four-storey frames): a) Beam sway; b) Mixed sway; c) Column sway; d) Mixed sway infilled. Note: the line type represents the conditioning damage state (DS_{MS}) while the line colour represents the achieved damage state (DS_{AS}). For example, the red dotted line represents $DS_{MS} = 1$ and $DS_{AS} = 4$. Gentile and Galasso (2021)

The mixed-sway frames (Figure 7.b), showing unstable hysteretic behaviour likely governed by shear failures in the joint panels, display a peculiar behaviour related to damage accumulation effects. For such an under-designed case study (that does not develop a soft-storey mechanism), the DS4|DS3 fragility median is 47% smaller than the DS4 median in the MS (12% reduction from DS2 to DS3|DS2). Given the higher median capacity with respect to the column-sway frames, damage accumulation is likely to be particularly relevant, in absolute terms, for this case study. This effect is amplified by the presence of the infills (Figure 7.d), which strongly govern the hysteretic behaviour of the frame for small displacements. In fact, a level of damage equal to DS3 corresponds to the (almost complete) degradation of the infills. As an approximation, if such a case study experiences a DS3 in the MS, it will behave as a bare frame in the AS. Indeed, the mixed-sway, infilled frame's DS4|DS3 median capacity is approximately equal to the DS4 median capacity of the corresponding

bare frame in the MS. In relative terms, the median capacity of the DS4|DS3 fragility is reduced by 70% with respect to the DS4 median capacity in the MS. The effect of the infills is qualitatively similar for the beam-sway and mixed-sway case studies. The column-sway pilotis frames are not discussed in detail since they effectively behave like the column-sway, bare frames (already discussed).

It is noted that each eight-storey case study is considerably less affected by damage accumulation if compared with the corresponding four-storey frame with the same properties. This is likely due to a loss of efficiency of $avgSA$ in the AS, with respect to the MS. In particular, the MS is likely to cause a period elongation of the structure, mainly affecting the vibration mode compatible with the developed plastic mechanism. In the AS, the relative influence of higher vibration modes changes with respect to the MS. Since the period range for $avgSA$ is based on undamaged conditions, period elongation causes the above-mentioned loss of efficiency of the IM.

5 CONCLUSION

This paper discussed a recent framework to derive state-dependent fragility relationships for structures subjected to mainshock-aftershock ground motion sequences. The total hysteretic energy dissipated in the ground-motion sequence is adopted as the main demand parameter in the proposed framework. Unlike peak parameters (e.g. maximum inter-storey drift), this allows one to develop statistical models consistent with the physics of a structure subjected to ground motion sequences.

It was proposed to use the median hysteretic energy vs peak deformation relationship for a given structure to convert the deformation-based damage state thresholds into energy-based ones. This allows calculating fragility relationships in energy terms while retaining the confidence of widely-accepted/calibrated deformation-based damage state thresholds.

A probabilistic seismic demand model was proposed in the form of a surface relating the hysteretic energy dissipated in the sequence to the peak deformation (e.g. maximum inter-storey drift) in the mainshock and an intensity measure of the aftershock (which may be a spectral acceleration or the geometric mean of the spectral acceleration in a range of periods). Such function is consistent with the relevant mechanics since the median hysteretic energy dissipated during the sequence is monotonic with respect to (any combination of) the maximum response in the mainshock and the intensity measure of the aftershock; and the hysteretic energy dissipated in the aftershock is lower if the peak deformation in the mainshock is higher. The proposed model may be considered a generalisation of the power-law relationship commonly adopted for cloud-based mainshock-only problems (it provides the same answer if it is used to predict mainshock fragility curves).

The results of an illustrative application involving 14 reinforced concrete frame buildings confirmed the feasibility of the proposed approach, which allows considering damage accumulation without inconsistencies in the statistical model. Furthermore, it is shown that, for a given structure, a sufficiently-large number of ground-motion records, with appropriate distributions of the geometric mean of the spectral acceleration and the significant duration, enables to fully characterise the structural response in energy terms, allowing one to capture the accumulation of damage.

6 ACKNOWLEDGEMENTS

This study is supported by the European Union's Horizon 2020 research and innovation programme under grant agreement No 821046, project TURNkey (Towards more Earthquake-resilient Urban Societies through a Multi-sensor-based Information System enabling Earthquake Forecasting, Early Warning and Rapid Response actions; *https://earthquake-turnkey.eu/*)

7 REFERENCES

Aljawhari, K., Freddi, F. and Galasso, C. (2019) 'State-dependent vulnerability of case-study reinforced concrete frames', in *COMPDYN 2019 - 7th ECCOMAS Thematic Conference on Computational Methods in Structural Dynamics and Earthquake Engineering*. Crete Island, Greece.

Carr, A. J. (2016) *RUAUMOKO2D - The Maori God of Volcanoes and Earthquakes. Inelastic Analysis Finite Element program.* Christchurch, New Zealand.

Chai, Y. H. (2005) 'Incorporating low-cycle fatigue model into duration-dependent inelastic design spectra', *Earthquake Engineering and Structural Dynamics*, 34(1), pp. 83–96. doi: 10.1002/eqe.422.

Changhai, Z. *et al.* (2018) 'Hysteretic energy prediction method for mainshock-aftershock sequences', *Earthquake*

Engineering and Engineering Vibration, 17(2), pp. 277–291.

Cosenza, E. and Manfredi, G. (2000) 'Damage indices and damage measures', *Progress in Structural Engineering and Materials*, 2(1), pp. 50–59. doi: 10.1002/(sici)1528-2716(200001/03)2:1<50::aid-pse7>3.3.co;2-j.

Decanini, L. D., Mollaioli, F. and Saragoni, R. (2000) 'Energy and displacement demands imposed by near-source ground motions', in *12th World Conference on Earthquake Engineering*. Auckland, New Zealand, pp. 1–8.

Fajfar, P. (1992) 'Equivalent ductility factors, taking into account low-cycle fatigue', *Earthquake Engineering & Structural Dynamics*, 21(10), pp. 837–848. doi: 10.1002/eqe.4290211001.

Gentile, R. *et al.* (2019) 'Non-linear analysis of RC masonry-infilled frames using the SLaMA method: part 2—parametric analysis and validation of the procedure [Open Access]', *Bulletin of Earthquake Engineering*, 17(6), pp. 3305–3326. doi: 10.1007/s10518-019-00584-6.

Gentile, R. and Galasso, C. (2021) 'Hysteretic energy-based state-dependent fragility for ground-motion sequences', *Earthquake Engineering & Structural Dynamics*, 50(4), pp. 1187–1203. doi: 10.1002/eqe.3387.

Housner, G. W. (1956) 'Limit design of structures to resist earthquakes', in *First World Conference on Earthquake Engineering*. San Francisco, California., pp. 1–13.

Jalayer, F. *et al.* (2017) 'Analytical fragility assessment using unscaled ground motion records', *Earthquake Engineering and Structural Dynamics*, 46(15), pp. 2639–2663. doi: 10.1002/eqe.2922.

Kircher, C. A., Whitman, R. V. and Holmes, W. T. (2006) 'HAZUS Earthquake Loss Estimation Methods', *Natural Hazards Review*, 7(2), pp. 45–59. doi: 10.1061/(asce)1527-6988(2006)7:2(45).

Kunnath, S. K. and Chai, Y. H. (2004) 'Cumulative damage-based inelastic cyclic demand spectrum', *Earthquake Engineering and Structural Dynamics*, 33(4), pp. 499–520. doi: 10.1002/eqe.363.

Malhotra, P. K. (2002) 'Cyclic-demand spectrum', *Earthquake Engineering and Structural Dynamics*, 31(7), pp. 1441–1457. doi: 10.1002/eqe.171.

NZS3101 (2006) 'Part 1: Concrete structures standard - The design of concrete structures. Wellington, New Zealand'. Wellington, New Zealand.

Papadopoulos, A. N., Kohrangi, M. and Bazzurro, P. (2020) 'Mainshock-consistent ground motion record selection for aftershock sequences', *Earthquake Engineering and Structural Dynamics*, (June 2019), pp. 754–771. doi: 10.1002/eqe.3263.

Priestley, M. J. N., Calvi, G. M. and Kowalsky, M. J. (2007) *Displacement-based seismic design of structures*. Pavia, Italy: IUSS Press.

Quinde, P., Terán-Gilmore, A. and Reinoso, E. (2019) 'Cumulative Structural Damage Due to Low Cycle Fatigue: An Energy-Based Approximation', *Journal of Earthquake Engineering*. doi: 10.1080/13632469.2019.1692736.

Terán Gilmore, A. (2001) 'Consideraciones De Uso De La Energía Plástica En El Diseño Sísmico (in spanish)', *Revista de Ingeniería Sísmica*, 110(65), p. 81. doi: 10.18867/ris.65.190.

Di Trapani, F. and Malavisi, M. (2019) 'Seismic fragility assessment of infilled frames subject to mainshock/aftershock sequences using a double incremental dynamic analysis approach', *Bulletin of Earthquake Engineering*. Springer Netherlands, 17(1), pp. 211–235. doi: 10.1007/s10518-018-0445-2.

Uang, C. -M and Bertero, V. V. (1990) 'Evaluation of seismic energy in structures', *Earthquake Engineering & Structural Dynamics*, 19(1), pp. 77–90. doi: 10.1002/eqe.4290190108.

Zhang, L. *et al.* (2020) 'Mainshock-aftershock state-dependent fragility curves: A case of wood-frame houses in British Columbia, Canada', *Earthquake Engineering and Structural Dynamics*, (July 2019), pp. 1–20. doi: 10.1002/eqe.3269.